

# Computational Study of Unsteady Flows around Dragonfly and Smooth Airfoils at Low Reynolds Numbers

H. Gao<sup>1</sup>, Hui Hu<sup>2</sup>, Z. J. Wang<sup>3</sup>

*Department of Aerospace Engineering, Iowa State University, Ames, IA, 50011*

A computational study was conducted to investigate the unsteady quasi-two-dimensional flow around a streamlined NASA low-speed GA(W)-1 airfoil and a corrugated dragonfly airfoil at the Reynolds numbers of 68,000 and 55,000. Both 2D and 3D simulations were carried out by solving the unsteady Navier-Stokes equations to predict the behavior of the unsteady flow structures around the airfoils at different angles of attack (AOAs). Extensive comparisons were made between the numerical results and wind-tunnel experimental results for the same configurations. It was found that the 2D and 3D simulations differ significantly at relatively high AOAs, and that the 3D computational results agree much better with the experimental data. It is believed that unsteady vortex-dominated flow at high angle of attack is strongly three-dimensional. As a result, the 2D simulations are not adequate in resolving the fundamental flow physics, and 3D simulations are necessary to correctly predict the flow behavior at such conditions.

## Nomenclature

$C_p$	=	pressure coefficient
$C_L$	=	lift coefficient
$Re$	=	Reynolds number
$Re_c$	=	chord-based Reynolds number
$c$	=	chord length
$t$	=	physical time
$\nu$	=	dynamic viscosity coefficient
$u$	=	velocity
$\omega$	=	vorticity
$x$	=	Cartesian coordinates
$p$	=	pressure
$i, j$	=	tensor indices

## I. Introduction

Low Reynolds number flow regime is the one where many Unmanned Aerial Vehicles (UAVs), and Micro-Air-Vehicles (MAVs) operate in, and recently, more and more attention has been paid to the study of aerodynamics of this regime. Although it usually refers to flows with chord based Reynolds number  $Re_c = 10,000 \sim 500,000$ , low Reynolds number flow is more often characterized by its flow features: normally a flow is said to be in low Reynolds number regime if it remains laminar until the onset of separation. And for particular angles of attack (AOAs), the flow will undergo a quick transition to turbulence and reattach to the airfoil surface, which is called a transitional separation bubble [1]. Low Reynolds number flows are often complicated since separation, transition and reattachment occur within a short distance and are said to be dominated by large scale vortex motions [2]. As a result, conventional airfoil designs for higher Reynolds number applications often have poorer performance at low Reynolds number regime [3].

---

<sup>1</sup> Graduate Student of Aerospace Engineering, 2271 Howe Hall, [hgao@iastate.edu](mailto:hgao@iastate.edu).

<sup>2</sup> Assistant Professor of Aerospace Engineering, 2271 Howe Hall, [huhui@iastate.edu](mailto:huhui@iastate.edu), AIAA Member.

<sup>3</sup> Associate Professor of Aerospace Engineering, 2271 Howe Hall, [zjw@iastate.edu](mailto:zjw@iastate.edu), Associate Fellow of AIAA.

Numerical studies of low Reynolds number flow started with 2D simulation with inviscid-viscous interaction methods [4, 5] and later full Navier-Stokes methods [6-10]. The challenge for low Reynolds number simulations is that the assumption that the whole flow field is turbulent is not valid for this flow regime. So normally certain transition prediction process needs to be used to turn on the turbulence model [10]. Another challenge is that standard turbulence models tend to work poorly in low Reynolds number flows. As a result, many special models are proposed and utilized [11, 12]. These studies focused on the time-averaged flow features and were able to obtain good agreements with experimental data up to the stalling AOA. However, most of them failed to work for higher AOAs.

Lin and Pauley (1996) [2] conducted an unsteady simulation of a 2D airfoil at a low Reynolds number, which revealed that underlying the attached time-averaged flow, there was a successive vortex shedding behavior near the trailing edge. The simulation agreed with Hu et al's PIV visualization [13]. In addition, an early incompressible Navier-Stokes (N-S) simulation was conducted in 2D with vorticity-streamfunction formulation of the N-S equations [14]. However, the post-stall trend is still not correctly predicted in either study.

Recently, Tamai et al. [15] and Hu et al. [13] have done extensive experimental studies on GA(W)-1 airfoil (Fig. 1) and corrugated dragonfly airfoil (Fig. 2). In both studies, the unsteady features of the flow were revealed, and the detailed measurement data make a good benchmark for the validation of the present numerical studies.

Most previous numerical studies are based on the 2D Navier-Stokes equations. But the question remains open whether the 2D simulation is sufficient to reveal the flow physics that is possibly dominated by large scale 3D structures, since a lot of these numerical simulations failed for high AOA cases. In the present study, both 2D and 3D numerical simulations were carried out and compared with experimental data. Through these comparisons, the validity of the 2D simulations at high AOAs is examined. It was found for high AOA flows, 3D simulations are necessary to correctly predict the flow in the stall regime.

## II. Numerical Methods

### A. Governing Equations and Flow Solvers

The governing equations are the unsteady 2D and 3D Navier-Stokes equations. All the numerical simulations in this study were mainly performed with the MUSIC code, a 2nd order finite volume flow solver capable of handling arbitrary meshes [16]. Although it was claimed in the PIV tests [13, 15] that turbulence existed in the separation regions and played an indispensable role in the reattachment of laminar separation, the computations in the present study were done with the Navier-Stokes equation without involving any turbulence models. This could be viewed as an implicit large eddy simulation (LES) simulation, in which the numerical dissipation serves as the sub-grid model. In order to verify some of the numerical simulations, several configurations were also simulated with a high-order spectral difference flow solver [17], and the commercial code Fluent. The use of different solvers in tackling the same configurations was designed to reduce numerical uncertainties involved in the simulations, and served to verify these simulations to some degree.

### B. Numerical Uncertainty Elimination

Given a perfect flow solver, there are still many uncertainties associated with the numerical simulations. The most well known one is the uncertainty with mesh resolution, which can be assessed with mesh refinement studies. Another important one for external flows is the size of the computational domain. For unsteady flow simulations, the size of the time step or CFL number, and the convergence tolerance used in the time step sub-iteration is also very critical. In order to build confidence in the numerical results, all uncertainties need to be minimized or eliminated if possible.

In the present study, a systematic way was employed to minimize the above uncertainties. For example, in order to choose the most economical domain size, numerical simulations were conducted with different domain sizes with other factors being identical. The smaller domain is roughly half of the size of the larger ones. If the computed lift coefficients differ by less than 1%, the size of the smaller domain is assumed adequate. Similar approaches were used to determine the time step, and the convergence tolerance. After that, a set of meshes with different resolutions were generated to use in the grid refinement studies. Some more details are presented next.

#### 1. Meshes

Three structured meshes for the GA(W)-1 airfoil and two for the dragonfly wing (Fig. 3) were constructed for grid refinement studies and simulations were performed on both set of meshes to study the effects of grid resolution.

#### 2. Boundary Conditions

First, the effect of the size of the computational was studied with several mesh configurations, after an appropriate domain size was chosen. Two types of inlet boundary conditions were applied at the inlet (fixing all

inflow variables and characteristic boundary condition or far field), and the results showed that as long as Reynolds number was maintained, the type of boundary condition did not cause noticeable differences.

### 3. Initial conditions

The experimental study on the same configurations showed no hysteresis effects [13, 15], which numerically means the solution should not be dependent on the initial conditions, and thus initial condition here was just taken as freestream.

### 4. Time integration

A second order accurate implicit backward difference scheme was used in time integration. The CFL number used and the inner convergence criteria were also carefully tested to confirm that no significant error was caused by these parameters.

### 5. Solver Verification

In addition to MUSIC, the FLUENT incompressible solver and a solver using 3rd order spectral difference method [17] were used to test several cases. If two solvers with two different numerical methods give similar solutions, there is a good chance that both solvers are correctly solving the flow problem.

## III. Numerical Results

### A. 2D Simulation for NASA GA(W)-1 Airfoil

The Reynolds number of this simulation is 64,000, the same as the experiment. According to [18], this Reynolds number yields unsteady flow at lower AOAs and separated 3D flow at higher AOAs.

The case with 10 deg AOA was chosen as the base case, where all the numerical verification studies were conducted to eliminate possible numerical errors. A set of meshes with different resolutions (coarse mesh: 320×80 cells, medium mesh: 640×160 cells, and fine mesh: 860×240 cells) were used in the mesh refinement study. The computed surface  $C_p$  distributions were displayed in Fig. 4. The computed lift coefficient histories using the MUSIC and FLUENT solvers on the medium mesh were shown in Fig. 5. It appears the results on the medium mesh agree well with those on the fine mesh, indicating the medium mesh is adequate. Note that also the two different solvers gave similar averaged lift coefficients, as shown in Figure 5. Then the 2D simulations were run for other AOAs on the medium mesh. The results for time-averaged lift coefficients are shown in Fig. 6. As can be seen, the computed lift coefficients agree well with experimental results at lower AOAs (under 7 deg), are mildly overestimated at mid-range AOAs (7-11 deg) where the flow is characterized by transitional separation bubbles. It is clear that the 2D simulations failed to predict stall at high AOAs (above 11 deg). In order to take a closer look at the flow fields, the pressure coefficients on the airfoil surface and the averaged streamlines for AOA of 6 degrees are shown in Figs. 7 and 8, and for AOA of 9 degrees displayed in Figs. 9 and 10 respectively. Note that at AOA of 6 degrees, the pressure coefficient agrees well with experimental data. Although a small separation bubble was predicted by CFD which did not appear in PIV measurement [15], it didn't seem to affect the pressure distribution a lot.

For the 9 deg AOA case, both the pressure distribution and average streamline comparison with the experiment suggested that the numerical simulations tended to predict longer separation bubble than that observed in the experiment, and this overprediction caused lift to be over-predicted too.

The most interesting cases were those at post-stall AOAs. None of the 2D simulations, either with MUSIC or FLUENT, on either the coarse or fine mesh predicted the stall phenomenon, as shown in Fig. 11, or the large separation region, which indicates 2D simulations are not capable of predicting stall. The computed averaged  $C_p$  profile on the airfoil surface is compared with the experimental measurement in Fig. 12. They are completely different! The suction peak near the leading edge remains intact while it has already collapsed from experimental data. The large separation region is nowhere to be seen. Instead, a small separation bubble is observed near the leading edge, as seen from the averaged streamlines shown in Fig. 13a This was quite different from PIV measurement, with a large separation zone above the airfoil.

This completely wrong 2D numerical solution seems independent of the mesh resolution and flow solver. Therefore, it is reasonable to conclude that 2D Navier-Stokes model itself is not capable of predicting stall at high AOAs. To further verify this, a 3D numerical study needs to be performed.

### B. 3D Simulation for NASA GA(W)-1 Airfoil

The 3D mesh was just an extrusion of the 2D coarse mesh, and due to the limit of computing power, the grid refinement study cannot be done as thoroughly as in 2D. The current study aims at resolving as much flow details as possible and revealing some of the effects of 3D structures. However, numerical tests were still done to determine the size of the spanwise direction and its resolution, and finally a reasonable mesh (with 320×80×41 cells and one chord length in the spanwise direction) was chosen to run all the simulations.

No spanwise disturbance was used to excite the 3D motion in this study, since the flow itself was so unstable that it could develop 3D structures out of numerical truncation errors from the time-stepping scheme in a short time.

First, the 16 deg AOA case was studied. When the lift coefficient history was compared with its 2D counterpart, the 3D simulation yielded much closer lift to the experimental average, as shown in Fig. 14. Furthermore, a completely different flow field is obtained with the 3D simulation, as shown in Fig. 13b, which displays the averaged streamlines. The 3D simulation was able to predict a large circulation zone which is very similar to PIV measurements. Therefore, the 3D simulation was capable of predicting the correct flow physics qualitatively even on the coarse mesh, unlike the 2D simulations.

The simulations at other AOAs were also performed, and the computed lift coefficients are shown in Fig. 6. The 3D simulations predicted a stall AOA of roughly 10 degrees, while 11 degree is the experimentally observed stall angle.

To explore the reason for the considerable difference at higher AOAs, the transient flow fields at AOA= 16 deg is examined more closely. In Fig. 15, the instantaneously vorticity distributions from the 2D and 3D simulations are compared. In the two-dimensional simulation, the vorticity was concentrated and located in a few very large vortex structures, and these large-scale vortices propagated in a path that is very close to the upper surface, and were never stationary. Whereas in a 3D simulation, concentrated vorticity only existed near the leading edge, after that, the vorticity is spread in the whole region above the airfoil resulting in a large recirculation region and no concentrated vortices were present.

The above observation seemed to suggest that the diffusion of the vorticity is completely different for 2D and 3D simulations. Explanation for this can be found from the vorticity transport equation (incompressible) below:

$$\frac{\partial \omega_i}{\partial t} + \left( u_j \frac{\partial}{\partial x_j} \right) \omega_i = \left( \omega_j \frac{\partial}{\partial x_j} \right) u_i + \nu \nabla^2 \omega_i.$$

For the 2D Navier-Stokes simulation, only one of the 3 equations above is valid, while in a 3D simulation, all three equations are valid, which means vorticity can diffuse in all three directions. In a 3D flow field, large vortices would be distorted and even intertwined by the growing three-dimensional disturbance, and would then break down to smaller scale structures in all the directions and be finally diffused to the whole region. This process also delivers energy to the smaller scale motions, and finally causes the transition to turbulence. However, in a 2D Navier-Stokes simulation, the vorticity is “trapped” in those 2D large vortex structures, and the diffusion of vorticity only happens around those vortices.

Therefore, it is speculated that in a real flow, the 3D structures cause the vorticity and the energy to diffuse to smaller scale motions, which form a large low speed area above the airfoil, and this prevents the pressure from building up from the trailing edge and thus cause the suction peak to collapse and the airfoil to stall (Fig. 16). While in 2D simulation the successive large vortices shedding behavior build a high speed zone (Fig. 17) near the surface, and the pressure is still allowed to build up.

However, at lower AOAs, as can be seen from Fig. 18, even if the flow is still 3D, the vorticity is mostly distributed near the surface instead of being diffused into a large area. In other words, the vorticity is also “trapped” and thus this behavior can be simulated in 2D, with minor discrepancies in the flow field (such as the small separation bubble near the trailing edge in Fig. 8). And based on this, the lift of lower AOA cases can be correctly computed using the 2D Navier-Stokes model.

For the mid-range AOAs, both 2D and 3D predicted longer separation bubble, but seemingly for different reasons: As is known, the reattachment is associated with the energy entrainment of smaller scale motions, and the results from 2D simulation is more or less a converged solution, and the lack of smaller scale motion is probably due to its incorrect energy diffusion behavior; while for 3D simulations, it is likely that the restriction of resolution that caused the lack of smaller scale motions, and this lack of ability to reattach is also a possible cause of the earlier separation predicted.

### C. Simulation of corrugated dragonfly airfoil

A similar simulation was performed on the corrugated dragonfly airfoil at  $Re_c= 55,000$ . In addition to all the above mentioned numerical verification, special attention was also paid to the sharp corners of the airfoil, since ideal sharp corners do not exist in any real case. Both sharp-corner and blunt-corner versions of the mesh were used but the results showed almost no difference.

Also, Fig.19 shows the mesh refinement and solver verification study at the AOA of 10 deg. This time, a 3rd order spectral difference solver was used to verify the results. As shown, the two solvers as well as the two meshes produced quite similar lift coefficients history.

Fig. 20 shows the final result of average lift coefficient from the 2D simulations. Not surprisingly, it shows a good agreement with experimental data at lower AOA, mild overestimation at mid-range AOA and the missing of stall behavior at higher AOA. And the large errors in post-stall behaviors should be again because of the incapability of 2D Navier-Stokes simulation.

Then the 3D simulation was conducted for the 16 deg AOA case, using both MUSIC and 3rd order spectral difference solver. Again, 3D simulation gave better agreement with the experiments, even with a coarser mesh (Fig. 21).

And when the transient vorticity field was examined in (Fig.22), the difference in vorticity diffusion is obvious: in the 2D simulation, vorticity is trapped in large vortex structures while in the 3D simulation, vorticity is diffused and broken into numerous smaller scale structures.

#### IV. Conclusion

Numerical results seem to indicate that 2D simulations are not adequate for the prediction of unsteady flow structures around the low-Reynolds-number airfoils at relatively high AOA with large scale separations. Since multiple 2D codes and methods were found to produce similar results, it is believed that the observation is not due to numerical uncertainties of the 2-D simulations. The incorrect vorticity diffusion behavior of 2D Navier-Stokes equation may be responsible for the significant difference found between the 2D and 3D simulation results. On the other hand, the 3D simulations appear to agree much better with experimental results, in both lift coefficients, and flow field characteristics, for both smooth and corrugated dragonfly airfoils. More simulations will be carried out to further verify this, especially mesh refinement studies in 3D. We believe that 2D simulations should not be recommended for the prediction of behavior of unsteady flow structures around low-Reynolds-number airfoils at high AOA.

#### Appendix

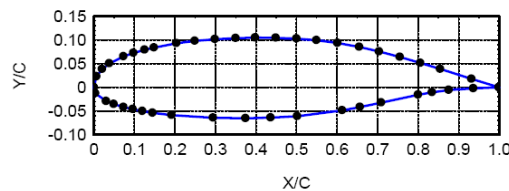


Figure 1. Streamliend NASA Low Speed GA(W)-1 airfoil

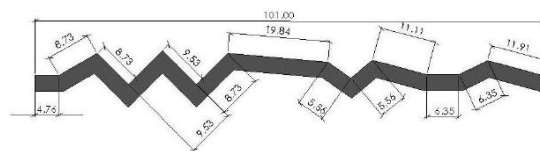


Figure 2. Corrugated dragonfly airfoil

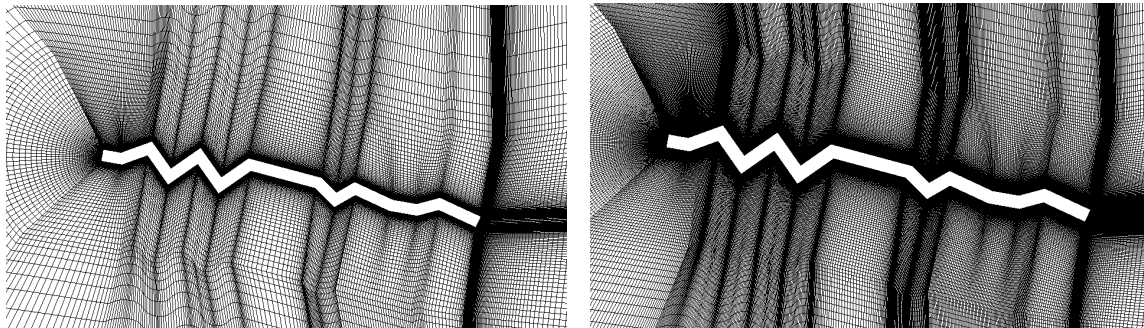


Figure 3. 2D Meshes for the Dragonfly Airfoil @ AOA=10deg. Coarse Mesh (left, 64408 cells) & Fine Mesh (right, 200208 cells)

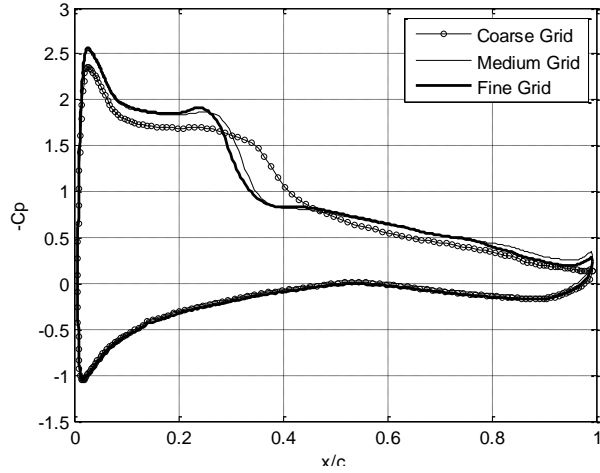


Figure 4.  $C_p$  Distribution on NASA GA(W)-1 Airfoil by Coarse, Medium and Fine Mesh @AOA=10 deg

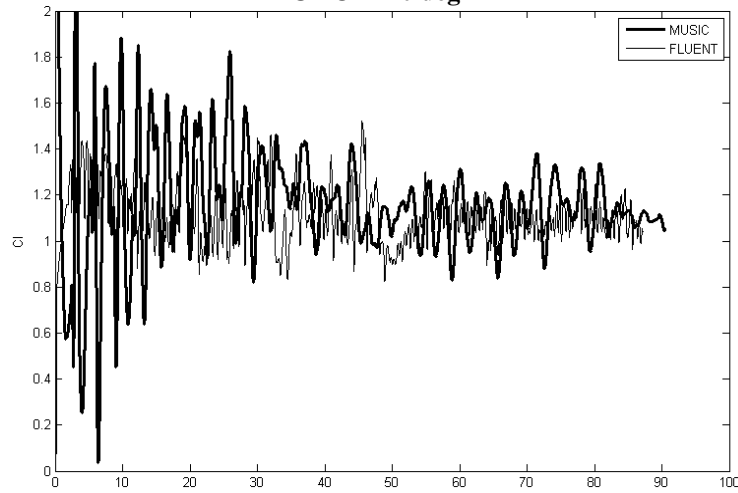


Figure 5. Lift Coefficient History of NASA GA(W)-1 Airfoil @AOA=10deg on the Medium Mesh

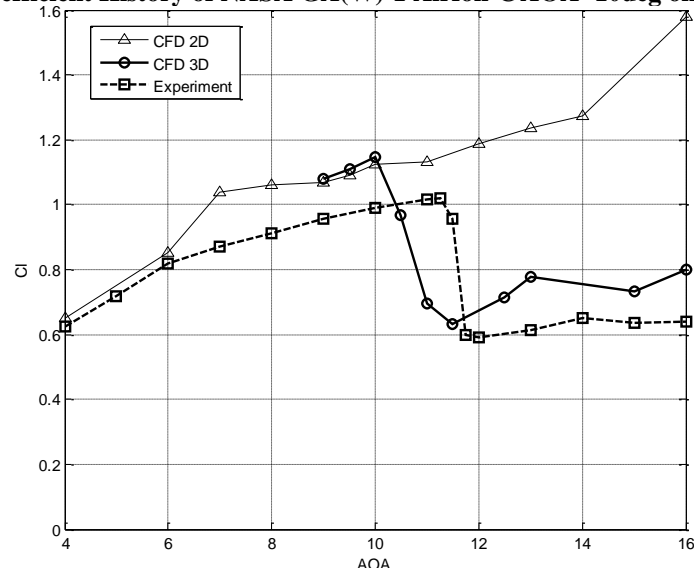


Figure 6. Lift Coefficient at Different AOAs from 2D & 3D simulation and Experiment of NASA GA(W)-1 Airfoil

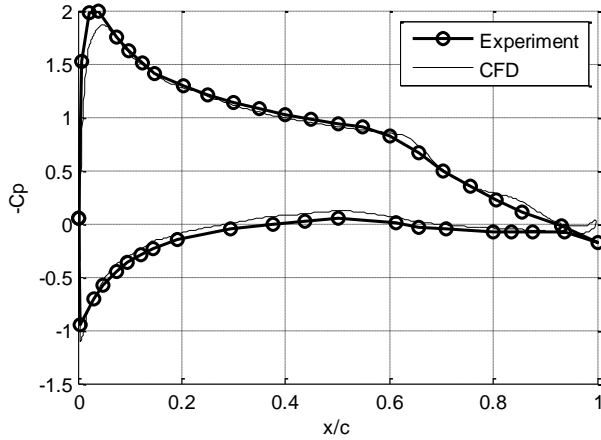


Figure 7. Airfoil Cp distribution @AOA=6 deg

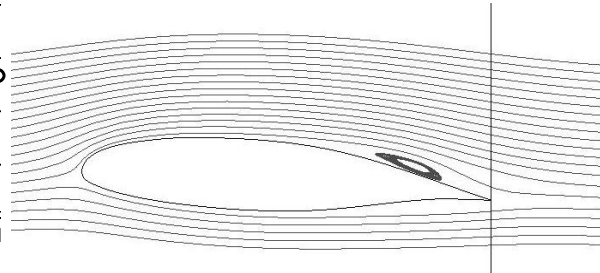


Figure 8. Airfoil Avg. Streamline @AOA=6 deg

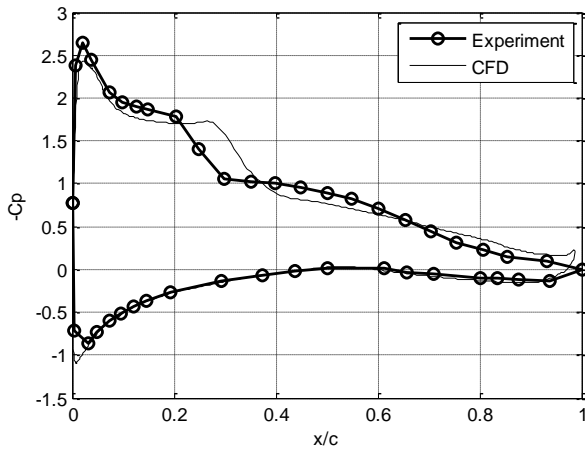


Figure 9. Airfoil Cp distribution @AOA=9 deg

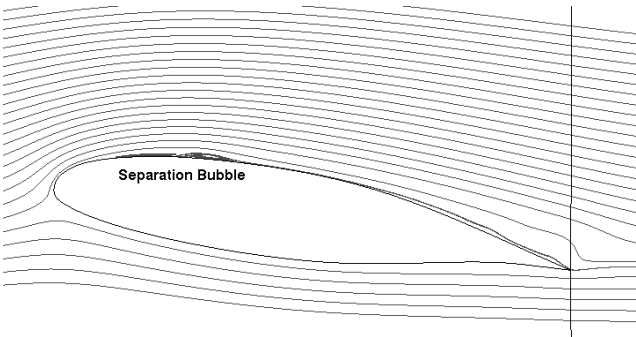


Figure 10. Airfoil Avg. Streamline @AOA=9 deg

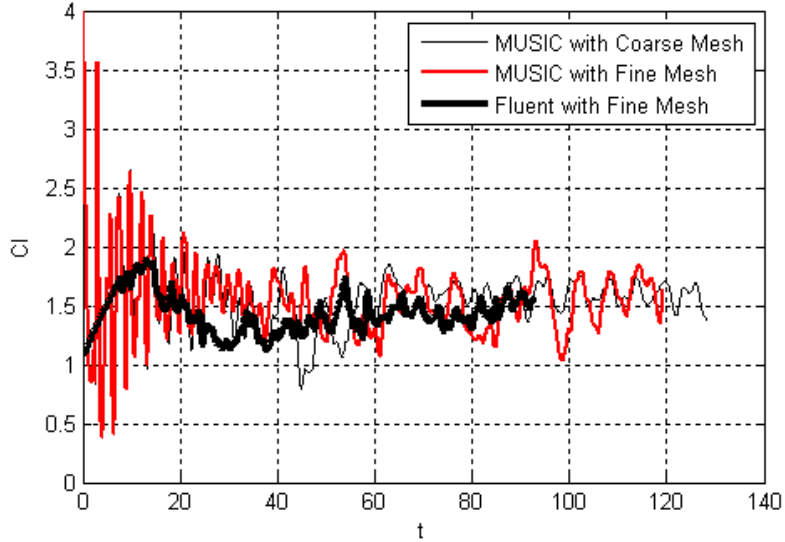


Figure 11. Lift Coefficients of NASA GA(W)-1 Airfoil @AOA=16 deg

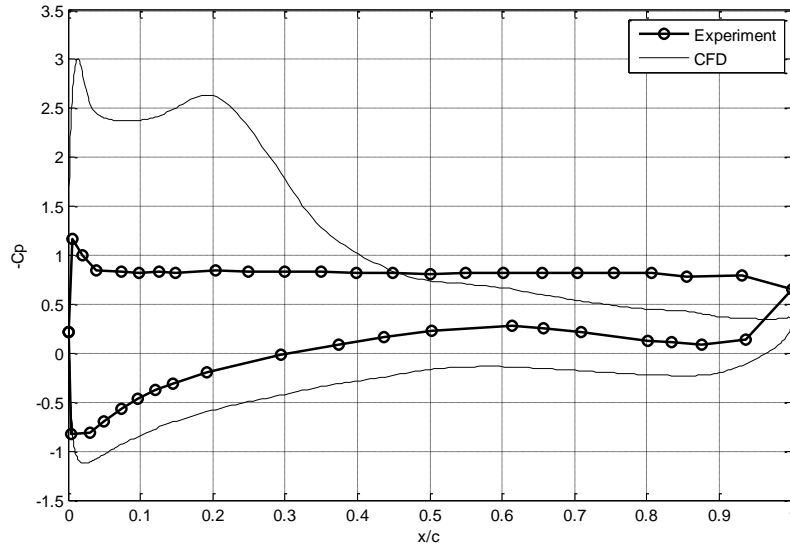
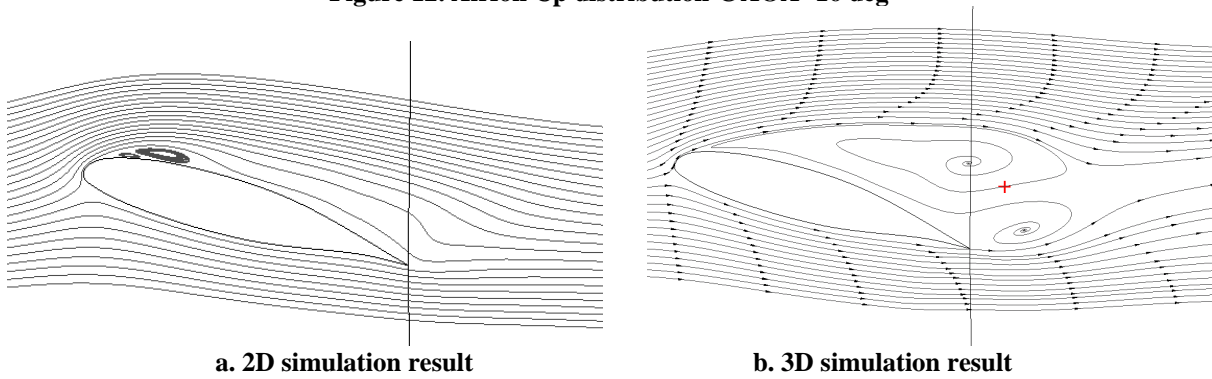


Figure 12. Airfoil Cp distribution @AOA=16 deg



a. 2D simulation result      b. 3D simulation result  
Figure 13. Mean flow field around the GA(W)-1 airfoil @ AOA=16deg

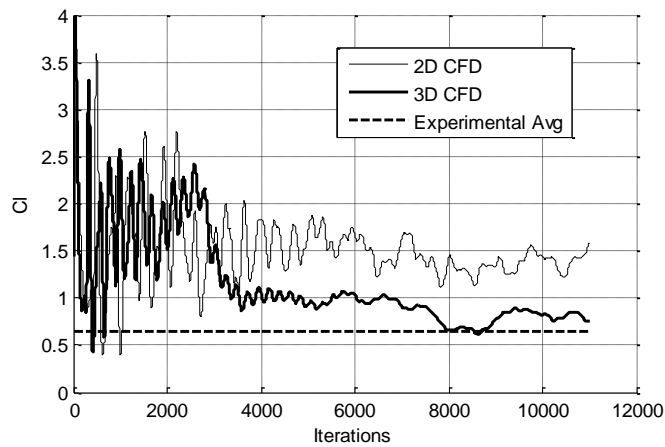
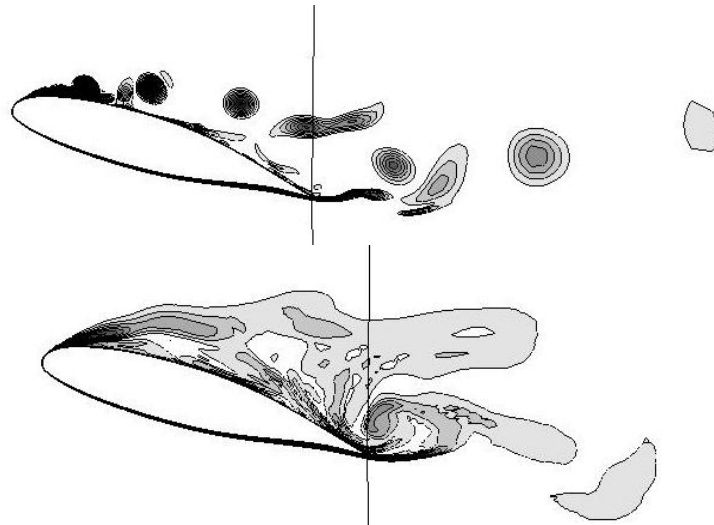
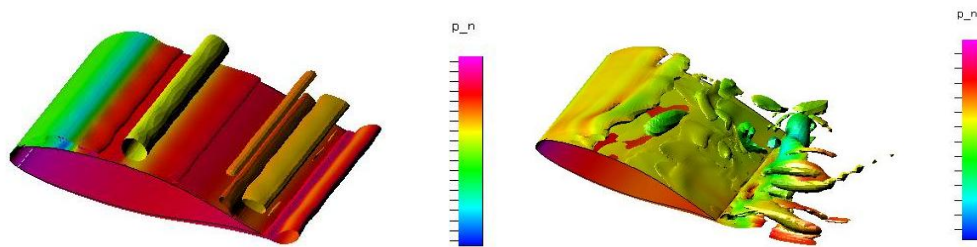


Figure 14.  $C_L$  history of NASA GA(W)-1 airfoil @AOA=16 deg



**Figure 15. Comparison of transient vorticity contours by 2D (top) simulation and 3D (bottom) simulation (median-span plane) @AOA=16 deg**



**Figure 16. Transient vorticity iso-surface colored by gauge pressure @AOA=16 deg. before (left) and after (right) 3D structures developed. The comparison shows the collapse of the low pressure area when flow becomes 3D and vorticity is diffused.**

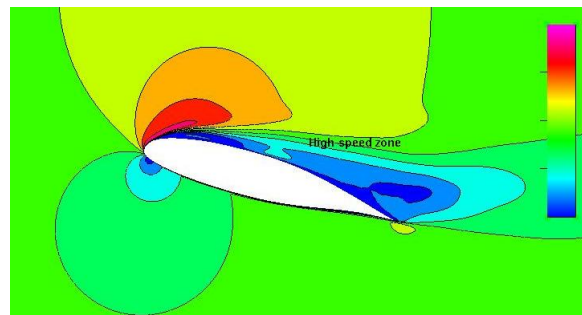


**Figure 17. Average velocity contours of airfoil @AOA=16 deg.**

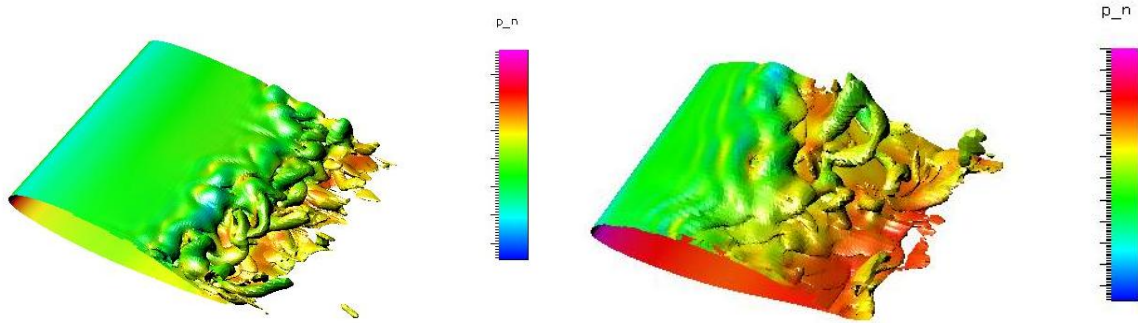


Figure 18. Transient vorticity iso-surface colored by gauge pressure: Left: @AOA=4 deg, Right: @AOA=10.

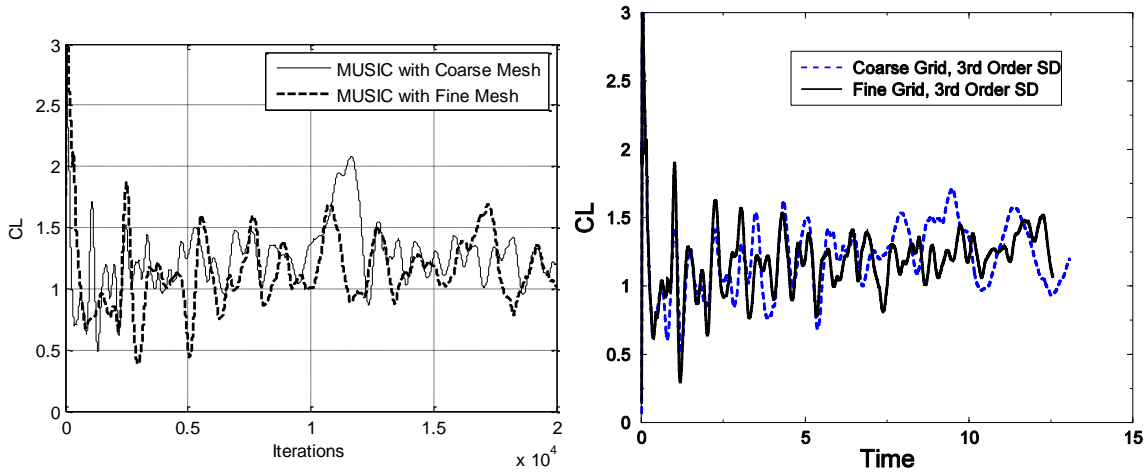


Figure 19.  $C_L$  of corrugated dragonfly airfoil @AOA= 10 deg. Solved by MUSIC and by 3<sup>rd</sup> order Spectral Difference solver.

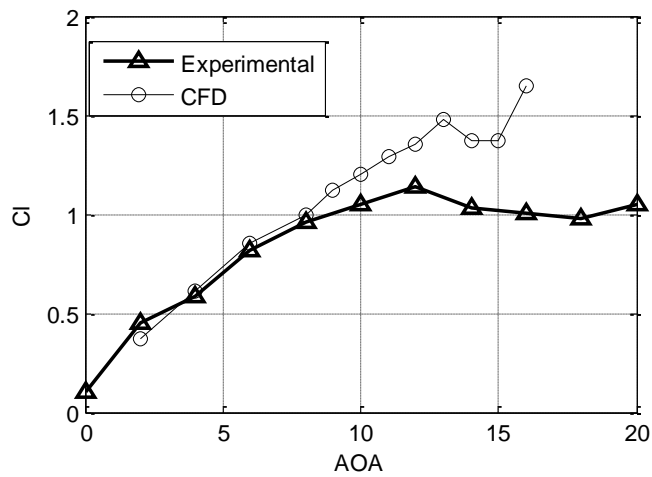
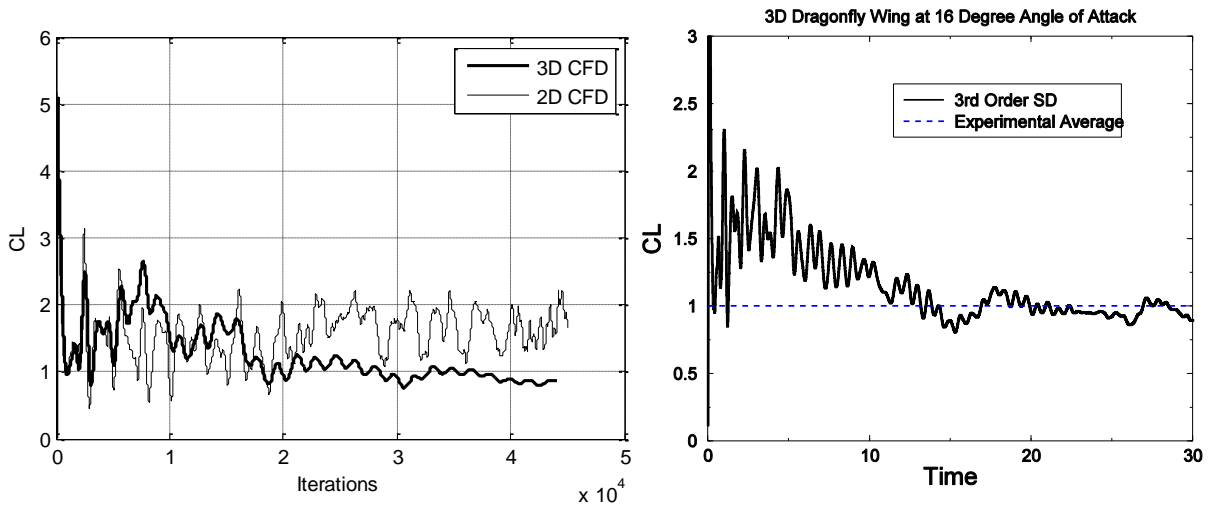
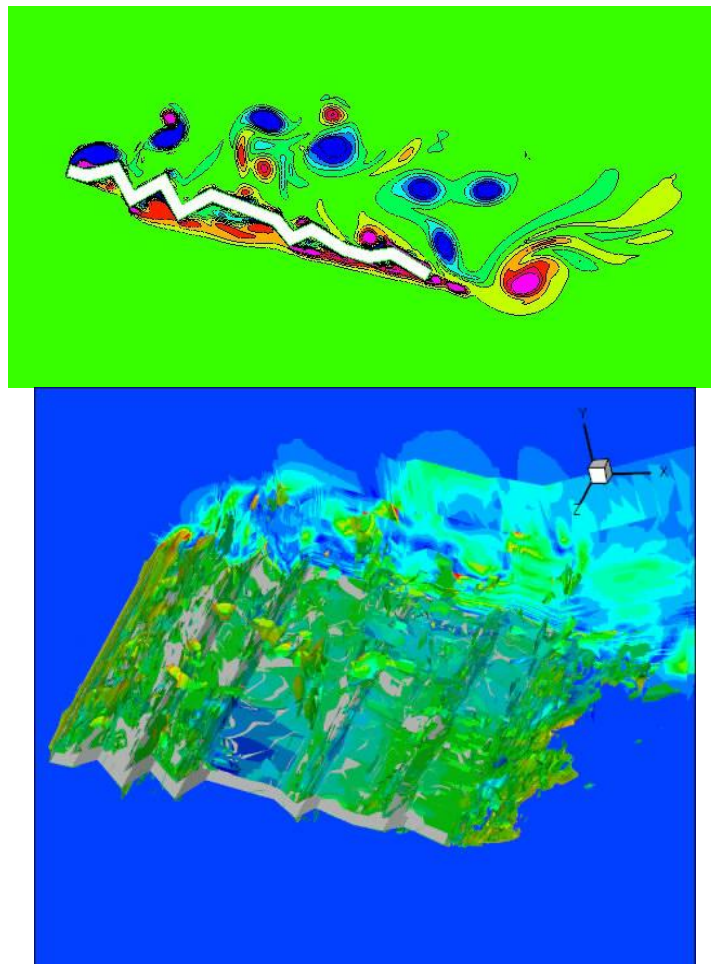


Figure 20.  $C_L$  Vs. AOA for dragonfly airfoil 2D simulation.



**Figure 21.**  $C_L$  of corrugated dragonfly airfoil @AOA= 16 deg. By MUSIC with 2D and 3D (Left) and Spectral Difference with 3D (Right).



**Figure 22.** Transient vorticity distribution of dragonfly airfoil @AOA=16 deg. Top: 2D simulation by MUSIC, Bottom: 3D simulation by 3rd order Spectral Difference

## References

- <sup>1</sup>Lissaman, P. B. S., "Low-Reynolds-Number Airfoils," Annual Review of Fluid Mechanics, Vol. 15, 1983, pp.223-239
- <sup>2</sup>Lin, J. C. Multi and Pauley, L. L., "Low-Reynolds-Number Separation on an Airfoil," AIAA Journal, Vol.34, No. 8, 1996, pp.1570-1577.
- <sup>3</sup>Schindel, L. H., "Store Separation," AGARD-AG-202, June 1975
- <sup>4</sup>Hsiao, F. B. and Hsu, C. C., "Numerical Prediction of Aerodynamic Performance for Low Reynolds Number Airfoils," Journal of Aircraft, Vol. 26, No.7, 1989, pp.689-692.
- <sup>5</sup>Coiro, D. P., "Prediction of Aerodynamic Performance of Airfoils in Low Reynolds Number Flows," *Low Reynolds Number Aerodynamics*, Springer, Berlin, 1989, pp.13-23.
- <sup>6</sup>Dini, P. and Maughmer, M. D., "Locally Interactive Laminar Separation Bubble Model," Journal of Aircraft, Vol. 31, No.4, 1994, pp. 802-810.
- <sup>7</sup>Cebeci, T., McIlvaine, M., Chen, H. H. and Liebeck, R. H., "Calculation of Low Reynolds Number Flows at High Angles of Attack," Journal of Aircraft, Vol. 28, No. 4, 1991, pp. 246-252.
- <sup>8</sup>Cebeci, T., Chen, H. H. and Lee, B. P., "Calculation of Three-Dimensional Low Reynolds Number Flows," Journal of Aircraft, Vol. 31, No. 3, 1994, pp. 564-571.
- <sup>9</sup>Shum, Y. K. and Marsden, D. J., "Separation Bubble Model for Low Reynolds Number Airfoil Applications," Journal of Aircraft, Vol. 31, No. 4, 1994, pp. 761-766.
- <sup>10</sup>Lian, Y. and Shyy, W., "Laminar-Turbulent transition of a Low Reynolds Number Rigid or Flexible Airfoil," AIAA Journal, Vol. 45, No.7, 2007, pp.1501-1513.
- <sup>11</sup>Chien, K. Y., "Predictions of Channel and Boundary-Layer Flows with a Low-Reynolds-Number Turbulence Model," AIAA Paper No. 80-0134R, 1980
- <sup>12</sup>Patel, V. C., Rodi, W. and Scheuerer, "Turbulence Models for Near-Wall and Low Reynolds Number Flows: A Reiview," AIAA Journal, Vol. 23, No. 9, 1985, pp. 1308
- <sup>13</sup>Hu, H. and Yang, Z., "An Experimental Study of the Laminar Flow Separation on a Low-Reynolds-Number Airfoil," Manuscript submitted to Journal of Fluid Engineering
- <sup>14</sup>Ghia, K. N., Osswald, G. and Ghia, U., "Study of Low-Reynolds Number Separated Flow Past the Wortmann FX 63-137 Airfoil," *Low Reynolds Number Aerodynamics*, Springer, Berlin, 1989, pp.58-69.
- <sup>15</sup>M. Tamai, Z. Wang, G. Rajagopalan, H. Hu, and G. He, Aerodynamic Performance of a Corrugated Dragonfly Airfoil Compared with Smooth Airfoils at Low Reynolds Numbers, 45th AIAA Aerospace Sciences Meeting and Exhibit, Reno, Nevada, Jan. 8-11, 2007
- <sup>16</sup>Z.J. Wang and R.F. Chen Anisotropic Solution Adaptive Viscous Cartesian Grid Method for Turbulence Flow Simulation, AIAA Journal, Vol. 40, No. 10, Oct. 2002
- <sup>17</sup>Sun, Y., Wang, Z.J. and Liu, Y., "High-Order Multidomain Spectral Difference Method for the Navier-Stokes Equations," AIAA-2006-0301.
- <sup>18</sup>Huang, R.F. and Lin, C.L., "Vortex shedding and shear-layer instability of wing at low-Reynolds numbers," AIAA Journal, Vol.33 (1995), pp. 1398-1430.